ELSEVIER

Contents lists available at ScienceDirect

Hybrid Advances

journal homepage: www.journals.elsevier.com/hybrid-advances



Research Article

Numerical computation of tangent hyperbolic magnetohydrodynamic Darcy–Forchheimer Williamson hybrid nanofluid flow configuring variable thermal conductivity

Jintu Mani Nath^a, Tusar Kanti Das^{b,*}, Ashish Paul^c, Ali J. Chamkha^d

- ^a Department of Mathematics, Mangaldai College, Mangaldai, 784125, India
- ^b Department of Mathematics, Dudhnoi College, Dudhnoi, 783124, Assam, India
- c Department of Mathematics, Cotton University, Guwahati, 781001, India
- ^d Kuwait College of Science and Technology, Doha District, 35004, Kuwait

ARTICLE INFO

Keywords: Darcy-Forchheimer Heat and mass transfer Williamson fluid Variable thermal conductivity Activation energy Tangent hyperbolic flow

ABSTRACT

The current investigation delves into the tangent hyperbolic Williamson hybrid nanofluid flow featuring varying thermal conductivity through the Darcy–Forchheimer medium across an exponentially stretching cylinder. Incorporating the activation energy and chemical reaction effects into consideration also strengthens the mathematical model's vitality. The considered hybrid nanofluid comprises silver and molybdenum disulfide nanoparticles submerged in the water. The highly non-linear system of equations is solved utilizing the MATLAB bvp4c approach. The influences of the leading variables versus involved fields are demonstrated through graphical delineations and tables. The core findings demonstrated that a strong Weissenberg number and Darcy-Forchheimer factor decay the velocity curve and strengthen the thermal curve. Also, the fluid concentration is enhanced for escalating activation energy and tangent hyperbolic factor. Additionally, the hybrid nanofluid betokens substantially enhance the thermal transportation rate of up to 8.8 % in contrast to nanofluid. Also, in contrast to the nanofluid and Williamson hybrid nanofluid, the hybrid nanofluid exhibits notably higher mass and thermal transport rate. This study is a noteworthy advancement in the disciplines of fluid dynamics and nanofluid research, as it provides promising potential for optimizing the transfer of mass and heat in a wide range of engineering and industrial contexts. The findings exhibit good agreement when contrasted with previously published work.

1. Introduction

The flow of fluid through a stretching cylinder is currently an area of great fascination among numerous researchers. A lot of engineering and commercial treatments are comprised of rubber sheet processing, heated tumbling, preparation, and manufacturing of paper, fabrication of glass fiber, etc. [1], exhibit boundary layer flows that are induced by stretching surfaces. Therefore, the movement of fluid through stretching cylinders is the primary issue of the scholarly community nowadays. Initially, Wang [2] gazed upon the fluid flow throughout a cylinder that was stretching. Furthermore, Khan et al. [3] computationally explored the flow of Carreau fluid across a stretched cylinder incorporating uniform and non-uniform reactions. They reported the fluid temperature augments for boosting the values of the curvature factor. Furthermore,

the repercussions of a magnetic dipole on the stream of a hybrid nanofluid through a stretching cylinder were addressed by Kumar et al. [4]. Their outcomes exposed that the increment in ferromagnetic interaction factor reduces the fluid velocity, but a reversal influence is indicated in thermal and mass distribution. After that, Paul et al. [5] computed numerically the heat transmission of MHD flow of $Cu - Al_2O_3/H_2O$ Casson hybrid nanofluid over a stretching cylinder considering the thermal source. They established that the hybrid Casson nanofluid fluid has a notable influence on the upsurge in the thermal processes. Recently, Othman et al. [6] computationally simulated the nanofluid flow incorporating activation energy and gyrotactic micro-organism impact over a stretching cylinder, which was inclined.

The current development in distinct scientific domains requires a pioneering revolution in the domain of thermal transmission. Enhancing

E-mail addresses: jmnath1995@gmail.com (J.M. Nath), tusarkantidas1995@gmail.com (T.K. Das), ashish.paul@cottonuniversity.ac.in (A. Paul), a.chamkha@kcst.edu.kw (A.J. Chamkha).

https://doi.org/10.1016/j.hybadv.2024.100343

Received 23 September 2024; Received in revised form 24 November 2024; Accepted 26 November 2024 Available online 27 November 2024

2773-207X/© 2024 The Authors. Published by Elsevier B.V. This is an open access article under the CC BY-NC-ND license (http://creativecommons.org/licenses/by-nc-nd/4.0/).

^{*} Corresponding author.

heat transmission is essential in the scientific and commercial sectors. In manufacturing processes, usual fluids like ethylene glycol and water serve as cooling solutions. Conventional fluids have poor thermal conductivity; therefore, even though adopting them can lower operating expenses, a boost in heat transfer is ineffective. Numerous investigators have recently become fascinated with nanofluid and hybrid nanofluid, which motivated them to enhance their computational and experimental research. Li et al. [7] addressed the efficacy of melting circumstances in the two-phase dusty carbon nanotube movement of Eyring-Powell fluid. Also, Zeeshan et al. [8] investigated the part of nano and hybrid nanofluid for elevating heat conductivity via exponentially elongating curves incorporating modified Fourier law. Furthermore, Li et al. [9] addressed the applications of Soret and Dufour impacts for Maxwell nanomaterial through convectively heated surfaces. The binary hybrid nanofluids are fluids that comprise two independent kinds of nanoparticles. The thermal transition of a hybrid nanofluid is considerably more notable than that of a typical nanofluid or any other fluid. The hybrid nanofluids have been used in a variety of operations, including refrigeration of electronic devices, welding, lubrication, temperature management of automobiles, production of drugs and papers, hydropower generation, etc. Maskeen et al. [10] explored the heat transport upsurge in hydromagnetic water-based $Al_2O_3 - Cu$ hybrid nanofluid flow across a stretching cylinder. According to their findings, single nanofluids and conventional fluids are less efficient at the transmission of heat than hybrid nanofluids. Moreover, across a stretched vertical cylinder, Waqas et al. [11] investigated the thermal transportation in the magnetized flow of hybrid nanofluids. They established that the greater values of the porosity factor decelerate the fluid flow while enhancing the thermal curve. Zainal et al. [12] looked at the unstable hybrid nanofluid flow of magneto-hydrodynamic flow. Their results confirmed that boosting the magnetic variable deteriorates the thermal features. Recently, Paul et al. [13] explored the MHD $Cu - Al_2O_3$ /water hybrid-nanofluid in a permeable domain over a stretched vertical cylinder combining thermal stratification. They illustrated that the shear rate of the hybrid nanofluid is larger in contrast with the nanofluid. Also, Nandi et al. [14] comparatively simulated the transient movement of hybrid nanofluid across a heated stretched cylinder incorporating velocity slip. Isa et al. [15] explored the Soret-Dufour influences on the water-driven hybrid nanofluid movement. Recently, Li et al. [16] theoretically studied the thermal and mass transport attributes of Al₂O₃/H₂O and (Al₂O₃+Ag)/H₂O nanofluids. Also, Mahmood et al. [17] numerically inspected the thermal transfer in radiative hybrid nanofluids via a moving sheet integrating porous media and slip conditions.

Magnetohydrodynamics (MHD) integrates fluid mechanics and electromagnetic concepts to study the dynamics of electrically conducting fluids in magnetic fields. By analyzing the effects of magnetic fields on fluid motion, MHD sheds light on intricate behaviors in conductive fluids such as liquid metals and plasma. To produce energy efficiently, high-temperature plasma is contained in reactors such as tokamaks using magnetic fields. This field is crucial to fusion energy. Additional uses include electromagnetic pumps for cooling liquid metal in reactors, magnetic propulsion systems for maritime vehicles, and astrophysical modeling that helps comprehend solar flares and the behavior of stellar atmospheres. Mukhopadhyay [18] studied the MHD boundary layer slip movement via a stretching cylinder. Furthermore, Reddy et al. [19] examined the impression of thermal absorption/generation on MHD thermal transmission fluid flow through an elongating cylinder incorporating a porous medium. Recently, Zhou et al. [20] explored the thermos-solutal Marangoni convective movement of MHD tangent hyperbolic hybrid nanofluids incorporating elastic deformation and thermal source. Also, Isa et al. [21] examined the Soret-Dufour influence on magnetohydrodynamics (MHD) Newtonian fluid movement via an inclined surface.

The boundary layer flow of fluids that are non-Newtonian underneath an extended cylinder is an intriguing scenario with numerous

implications for scholars. Its applications incorporate the expulsion process, metal mining, heating, copper wire flattening, and pipeline fabrication. Non-Newtonian fluids presently dominate Newtonian fluids in the majority of industries. The conventional Naiver-Stokes models struggle to explicate the rheological traits of non-Newtonian fluids. Furthermore, a single model is incapable to represent the properties of non-Newtonian fluids. There have been several models put forth for tackling this problem. The Williamson fluid paradigm was initially proposed by Williamson [22] and is reflective of a non-Newtonian fluid exhibiting shear retreating behavior. Also, Bilal et al. [23] attempted a numerical assessment of MHD and heat radiation on Williamson nanofluid movement underneath a stretching cylinder involving varying heat conductivity. They established that the profile of velocity diminishes as the Weissenberg number boosts, whereas the thermal curve displays the reverse relationship. Also, incorporating the impact of activation energy, Ibrahim et al. [24] explored the Williamson nanofluid across a stretched cylinder. They reported that the flow speed decelerates whereas the thermal and concentration curves improve when the porous variable is accelerated. Moreover, the bio-convection radiative stream of Williamson nanofluid through a stretched cylinder incorporating activation energy was computationally simulated by Zhang et al. [25]. They concluded that elevating Darcy-Forchheimer shrinks the thickness of the boundary layer of momentum and the fluid velocity. Meanwhile, Rashad et al. [26] explored the heat fluctuation on MHD Williamson hybrid nanofluid movement in conjunction with convective boundary constraints and Ohmic heating.

An adaptable fluid mechanism, Tangent Hyperbolic Hybrid nanofluid Flow, is focused mainly on enhancing temperature management and the transfer of heat in various procedures and systems. It has intriguing uses across numerous domains. Tangent Hyperbolic Hybrid nanofluid flow can be utilized in situations where accurate temperature regulation, improved exchange of heat, and optimized fluid flow are important. Upgraded heat exchangers, solar energy systems, electronic cooling, biomedical devices, and environmental engineering are a few examples of potential applications. Salahuddin et al. [27] addressed the implications of temperature generation/absorption on tangent hyperbolic nanofluid approaching the stagnation point across an expanding cylinder. The model they developed throughout their research incorporated tangent hyperbolic nanofluid flow, Brownian motion, and thermophoresis impacts. The findings indicate that the rate of shear and heat transport at the surface strengthens while nanoparticles are integrated into the tangent hyperbolic fluid. Following that, the irregular magnetohydrodynamic flow of tangent hyperbolic nanofluid across a cylinder incorporating Brownian motion effects was investigated by Gharami et al. [28]. Moreover, Kumar et al. [29] numerically simulated the thermal radiation and nanoparticle size, incorporating the magnetic field influence, depending on the stream of tangent hyperbolic nanofluid. They reported that the friction drag, heat layer, and micro-rotation all lessen when the radial size of the nanoparticles is enhanced. Recently, in a mixed convection system together with recurrent magneto-hydrodynamics, Patil et al. [30] assessed the movement of a tangent hyperbolic ternary hybrid nanofluid around a rough-yawed cylinder driven by impulsive motion.

A significant number of researchers have been devoting special attention to the Darcy-Forchheimer porous effect during that period. A lot of research has been conducted concerning heat and transmission of mass, yet when it pertains to Darcy-Forchheimer flow via a stretched cylinder, there is plenty to be explored with a reliable and precise computational method. Ultra-filtering techniques in drug companies, significant contamination of water in indigenous reservoirs, and the shipping of commercial wastes are a few real applications of the Darcy-Forchheimer impact. Saeed et al. [31] demonstrated the Darcy hybrid nanofluid flow and thermal transport investigation across a porous stretched cylinder. Furthermore, the impact of activation energy and chemical reactions on the MHD flow of Williamson nanofluid in a Darcy-Forchheimer porous medium was examined by Gautam et al.

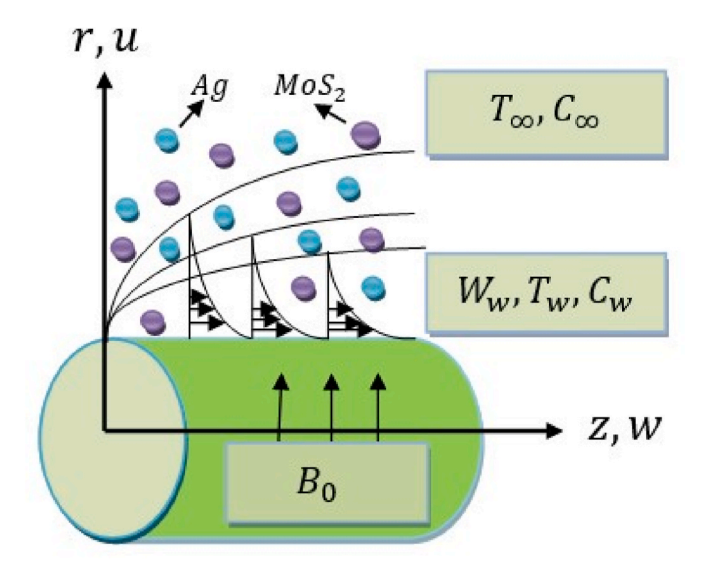


Fig. 1. Physical demonstration of the proposed model.

[32]. According to their study outcomes, the exterior drag force improves with the magnetic component but lowers with the Williamson variable. Moreover, computational coursework on the MHD hybrid Darcy nanofluid circulation subject to the impacts of activation energy and chemical reactions throughout an extending surface was conducted by Haq et al. [33]. They established that Darcy–Forchhemier's influence notably reduced the thermal transmission rate of hybrid nanofluids. Recently, Alqahtani et al. [34] observed the thermal and mass transport influence through the circulation of Darcy Forchheimer MHD Casson hybrid nanofluid through an exponential stretched sheet. Moreover, Li et al. [35] investigated the consequence of mutable fluid features on combined convective Darcy–Forchheimer flow. Also, Enamul and Ontela [36] addressed the MHD Darcy-Forchheimer movement of non-Newtonian second-grade hybrid nanofluid integrating varying heat conductivity and Entropy generation.

Svante Arrhenius pointed out the concept of "activation energy" in 1889, and it entails a minimal quantity of energy that molecules or particles require to acquire to start a chemical process. Water-and-oil emulsions, the processing of food, and other domains all demand activation energy and chemical reactions that involve the transport of mass. Shanmugapriya et al. [37] significantly observed the thermal and mass transmit upsurge of MHD hybrid nanofluid flow incorporating activation energy. Their findings illustrated that the nanoparticle transmission rate of the hybrid nanofluid accelerates as the activation energy improves. After that, Azam et al. [38] looked into the irregular thermal flux of Williamson nanofluid in conjunction with the energy of activation, and gyrotactic microorganisms. Also, the significance of activation energy and a varying thermal source on the electro-magnetohydrodynamic flow of hybrid nanofluid across a movable stretchable disc with nonlinear radiation was analyzed by Kumar et al. [39]. They demonstrated that fluctuations in the volume proportion of copper and magnetite nanoparticles are inversely correlated with velocity. Furthermore, Puneeth et al. [40] explored the stratified bio-convective jet flow of Williamson nanofluid in a permeable space in the existence

Table 1Hybrid nanoparticles' and the base fluid's thermo-physical attributes Ref.[49, 50]

Properties	MoS_2	Ag	H_2O (Base fluid)
$\rho \left(kg/m^{3}\right)$	5060	10490	997.1
$c_p (J/kgK)$	397.21	235	4179
k(W/mK)	904.4	429	0.6130
$\sigma(S/m)$	2.09×10^4	6.30×10^7	0.05

of Arrhenius energy. Recently, Saini et al. [41] demonstrated the activation energy, convective thermal transmission, and Joule heating impact on the radiative Williamson nanofluid flow across a radially stretched sheet. They established that the activation energy factors have proportional impacts on the concentration curve. Recently a few researchers [42–46] have investigated experimentally and numerically and obtained outstanding findings in the field of fluid dynamics.

This investigation examines the flow characteristics of a tangent hyperbolic Darcy-Forchheimer Williamson hybrid nanofluid over an exponentially stretching cylinder. The research is novel in its consideration of Arrhenius activation energy, chemical reaction effects, and variable thermal conductivity on the water-based Ag/MoS₂ Williamson nanofluid. Despite the fluid's substantial industrial relevance, previous studies have yet to explore these influences within an exponentially stretched cylinder geometry. This unique focus provides a significant new perspective on fluid behavior in complex geometries, enhancing understanding of such hybrid nanofluid dynamics. This study used Silver (Ag) and molybdenum disulfide (MoS₂) as nanoparticles and Water as a base fluid. The amalgamation of silver and molybdenum disulfide (MoS₂) nanoparticles dispersed in water has shown superior performance, due to their unique synergistic features and elevated thermal conductivity. Silver nanoparticles are extremely conductive, which upsurges the thermal transfer capability, while MoS2 provides excellent lubricating attributes and stability in aqueous solutions, lessening particle agglomeration and boosting overall dispersion. Water, as a base fluid, has high specific heat, allowing for effective heat energy transmission. The current study also performed a comprehensive comparison of three different fluid flow circumstances, including the flow of nanofluid, hybrid nanofluid, and Williamson hybrid nanofluid. The comparisons focused on the skin friction coefficients, heat, and mass transfer rates of all three scenarios. Thus, this work forges a new and creative route in the discipline, bringing with it a plethora of practical implications and bringing in academics and industry operators keen to use these revolutionary findings to foster creativity and effectiveness across a range of manufacturing procedures. This model has broad applications in a variety of domains, such as the automotive industry, solar thermal systems, microfluidics, medical equipment, nuclear reactors, and the aerospace sector. Also, this model provides intriguing prospects for optimizing the transportation of heat and mass in a variety of industrial settings and engineering domains.

2. Mathematical formulation

In this study, based on the boundary layer approach and steady laminar flow phenomenon, we have considered two-dimensional tangent hyperbolic Ag - MoS₂/H₂O Williamson hybrid nanofluid flow over an exponentially stretching cylinder in the existence of chemical reaction. This flow problem is considered the cylindrical polar (z, r)coordinate system, in which z specifies axial direction and r specifies radial direction. As indicated in Fig. 1, this flow is addressed by induced Lorentz force (B_0) in the convective flow domain and the exponentially stretching surface is taken to move through the velocity $w_w =$ $2ac \exp\left(\frac{z}{a}\right)$, where c and a emblematize the stretching rate and base radius of the cylinder respectively. The wall temperature (T_w) and wall concentration (C_w) are considered as $T_w = T_\infty + A^* \exp\left(\frac{z}{a}\right)$ and $C_w =$ $C_{\infty} + B^* \exp\left(\frac{z}{a}\right)$, where A^* , B^* , T_{∞} and C_{∞} symbolizes the non-negative constants, ambient temperature, and concentration, respectively. Also, the impacts of activation energy, Darcy-Forchheimer media, and variable thermal conductivity are taken in this flow phenomenon. The variable thermal conductivity is considered to be varied with temperature as $k_{hnf}(T) = k_{hnf}(1 + \epsilon \theta(\eta))$, where ϵ is indicated as a variable thermal conductivity parameter.

By employing the aforementioned supposition, the constitutive

governing equations become the following (Ref. [23,47,48])::

Continuity Equation

$$\frac{\partial u}{\partial r} + \frac{u}{r} + \frac{\partial w}{\partial z} = 0 \tag{1}$$

Momentum Equation

$$(1 + \epsilon\theta)(\eta\theta'' + \theta') + \epsilon\eta\theta'^2 = \frac{(\rho C_p)_{hnf}}{(\rho C_p)_f} \left(\frac{k_f}{k_{hnf}}\right) Pr.Re(f'\theta - f\theta') \tag{7}$$

$$\eta \phi'' + \phi' = Re.Sc(f'\phi - f\phi') + Re.Sc.Cr(1 + \gamma\theta)^N \exp\left(-\frac{E}{1 + \gamma\theta}\right)\phi$$
 (8)

$$u\frac{\partial w}{\partial r} + w\frac{\partial w}{\partial z} = \frac{\mu_{hnf}}{\rho_{hnf}} \left[(1 - m) \left(\frac{\partial^2 w}{\partial r^2} + \frac{1}{r} \frac{\partial w}{\partial r} \right) + m\Gamma\sqrt{2} \right] \frac{\partial w}{\partial r} \left(\frac{\partial^2 w}{\partial r^2} \right) + \frac{m\Gamma}{\sqrt{2}r} \left(\frac{\partial w}{\partial r} \right)^2 \right] - \frac{\sigma_{hnf}}{\rho_{hnf}} B_0^2 w - \frac{\mu_{hnf}}{\rho_{hnf}} \frac{1}{k_p} w - \frac{c_b}{\sqrt{k_p}} w^2$$

$$(2)$$

Here.

The converted boundary constraints are

Energy Equation

$$u\frac{\partial T}{\partial r} + w\frac{\partial T}{\partial z} = \frac{1}{r}\frac{\partial}{\partial r}\left(k_{hnf}(T)r\frac{\partial T}{\partial r}\right)$$
(3)

Concentration Equation

$$f(1) = 0, f'(1) = 1, \theta(1) = 1, \phi(1) = 1$$
 (9)

 $f(\infty) = 0, \theta(\infty) = 0, \phi(\infty) = 0$ (10)

$$Pr = \frac{v_f}{\alpha_f}, Re = \frac{aw_w}{4v_f}, We = \frac{2\sqrt{2\Gamma}w_w}{a}, M = \frac{\sigma_f B_0^2 a}{\rho_f w_w}, \alpha_f = \frac{K_f}{\left(\rho C_p\right)_f}, Cr = \frac{K_r^2 a}{w_w}, E = \frac{E_a}{K_1 T_\infty}, \gamma = \frac{T_w - T_\infty}{T_\infty}, Sc = \frac{v_f}{D_f}, Fr = \frac{c_b a}{\sqrt{k_p}}, P = \frac{a^2}{4k_p}$$

$$u\frac{\partial C}{\partial r} + w\frac{\partial C}{\partial z} = D\left(\frac{1}{r}\frac{\partial C}{\partial r} + \frac{\partial^2 C}{\partial r^2}\right) - k_r^2(C - C_\infty)\left(\frac{T}{T_\infty}\right)^N \exp\left(\frac{E_a}{K_1 T}\right)$$
(4)

Along boundary constraints are [5,27].

$$w(a,z) = w_w, u(a,z) = 0, T(a,z) = T_w(z), C(a,z) = C_w(z)$$
 at $r = a$

$$w(r,z) \to 0, T(r,z) \to 0, C(r,z) \to 0 \text{ at } r \to \infty$$
 (5)

Here (u,w) indicates the velocity components run along (r,z) direction. The activation Arrhenius parameter $k_r^2 \left(\frac{T}{T_\infty}\right)^N \exp\left(\frac{Ea}{K_1T}\right)$ is addressed in the concentration equation with the Boltzmann constant K_1 , where -1 < N < 1.

The similarity transformation variables, we have used here are as follows (Ref. [5]):

$$\eta = \left(\frac{r}{a}\right)^2, w = w_w f(\eta), u = -\frac{1}{2} w_w \frac{f(\eta)}{\sqrt{n}}$$

$$\theta = \frac{T - T_{\infty}}{T_{\infty} - T_{\infty}}, \phi = \frac{C - C_{\infty}}{C_{\infty} - C_{\infty}}$$

After the use of the non-dimensional similarity variables mentioned above, the transformed coupled ordinary differential equations (ODEs) can be demonstrated as follows:

Where, $Pr, Re, We, M, \alpha_f, Cr, E, \gamma, Sc, Fr$ and P indicates Prandtl number, Reynolds number, Weissenberg number, magnetic factor, thermal diffusivity, chemical reaction term, activation energy, temperature ratio parameter, Schmidt number, Darcy-Forchheimer, and porosity parameter respectively.

The physical variables of scientific concern in this flow problem are the coefficient of drag force, Nusselt, and Sherwood number, which physically indicate the tangential stress, the rate of thermal transmission, and the rate of mass transport at the surface respectively.

Skin Friction coefficient:

$$\tau_{w} = \mu_{hnf} \left((1 - m) \frac{\partial w}{\partial r} + \frac{m\Gamma}{\sqrt{2}} \left(\frac{\partial w}{\partial r} \right)^{2} \right)$$

Nusselt Number:

$$Nu_z = rac{aexp\left(rac{z}{a}
ight)q_w}{k_f(T_w - T_\infty)}$$
, where $q_w = -k_{hnf}(T)\left(rac{\partial T}{\partial r}\right)_{r=a}$

Sherwood Number:

$$Sh_z=rac{aexp\left(rac{z}{a}
ight)q_m}{D(C_w-C_\infty)}$$
 , where $q_m=D\left(rac{\partial C}{\partial r}
ight)_{r=a}$

By imposing the similarity transformation variables the transformed skin, nusselt, and Sherwood number (Ref. [29,30]) can be rewritten as:

$$C_f Re_z^{\frac{1}{2}} = \frac{\mu_{hnf}}{\mu_f} \left[(1-m)f''(1) + m \frac{We}{2}f''(1)^2 \right]$$

$$f'^{2} - ff'' = \frac{1}{Re} \frac{\mu_{hnf}}{\mu_{f}} \frac{\rho_{f}}{\rho_{hnf}} \left[(1 - m)(\eta f''' + f'') + m.We.\sqrt{\eta} \left(\eta f'' f''' + \frac{3}{4} f''^{2} \right) \right] - \frac{\sigma_{hnf}}{\sigma_{f}} \frac{\rho_{f}}{\rho_{hnf}} M.f - \frac{\mu_{hnf}}{\mu_{f}} \frac{\rho_{f}}{\rho_{hnf}} \frac{P}{Re} f' - Fr.f'^{2}$$

$$(6)$$

$$extit{Nu}_{z} extit{Re}_{z}^{-rac{1}{z}} = -\left(rac{ extit{K}_{hnf}}{ extit{K}_{f}}(1+\epsilon heta(1))
ight) heta'(1)$$

Table 2
Comparable findings with Wang [55] and Ishak et al. [56]

Re	Wang [55]	Ishak et al. [56]	Present study
0.5	-0.88220	-0.8827	-0.8824
1	-1.17776	-1.1781	-1.1778
2	-1.59390	-1.5941	-1.5939
5	-2.41745	-2.4175	-2.4174
10	-3.34445	-3.3445	-3.3445

 Table 3

 Indication of greater heat transmission through some experimental investigation.

References	Used Nanoparticles	Type of Investigation	Findings
Zhang et al. [57]	MoS_2	Experimental	The experimental result indicates that the addition of nanoparticles in the palm oildriven base fluid produced the best lubricating property. Furthermore 6 % mass fraction was identified to be the optimal addition concentration for MoS ₂ nanoparticle.
Mousavi et al. [58]	MoS_2	Experimental	The pumping power and friction faction was enhanced by the incorporation of <i>MoS</i> ₂ nanoparticle.
Godson et al. [59]	Ag	Experimental	A minimum and maximum enhancement of 27 % at 0.3 vol% and 80 % at 0.9 vol% are reported at an average temperature of 70 °C.

$$\mathit{Sh}_{z}\mathit{Re}_{z}^{-\frac{1}{z}}=-\phi'(1)$$

Table 1 displays the hybrid nanoparticles and the base fluid's thermo-physical attributes.

THE EMPIRICAL CORRELATIONS FOR HYBRID NANOFLUID (Ref. [51,52]).

• Density

$$\rho_{\mathit{hnf}} = (1 - \phi_2) \big\{ (1 - \varphi_1) \rho_{\mathit{f}} + \phi_1 \rho_{\mathit{s}1} \big\} + \phi_2 \rho_{\mathit{s}2}$$

• Specific heat capacity

$$\left(\rho C_{p}\right)_{\mathit{hnf}} = (1-\phi_{2}) \Big\{ (1-\phi_{1}) \big(\rho C_{p}\big)_{f} + \phi_{1} \big(\rho C_{p}\big)_{\mathit{s}1} \Big\} + \phi_{2} \big(\rho C_{p}\big)_{\mathit{s}2}$$

• Dynamic viscosity

$$\mu_{hnf} = \frac{\mu_f}{(1 - \phi_1)^{2.5} (1 - \phi_2)^{2.5}}$$

· Thermal conductivity

$$\frac{k_{nf}}{k_{f}} = \left\{ \frac{k_{s1} + 2k_{nf} - 2\phi_{s1}(k_{nf} - k_{s1})}{k_{s1} + 2k_{nf} + \phi_{1}(k_{nf} - k_{s1})} \right\}$$

$$\frac{k_{hnf}}{k_{nf}} = \left\{ \frac{k_{s2} + 2k_f - 2\phi_2(k_f - k_{s2})}{k_{s2} + 2k_f + \phi_2(k_f - k_{s2})} \right\}$$

• Electric conductivity:

$$\frac{\sigma_{nf}}{\sigma_{f}} = \left\{ \frac{\sigma_{s1} + 2\sigma_{f} - 2\phi_{1}(\sigma_{f} - \sigma_{s1})}{\sigma_{s1} + 2\sigma_{f} + \phi_{1}(\sigma_{f} - \sigma_{s1})} \right\}$$

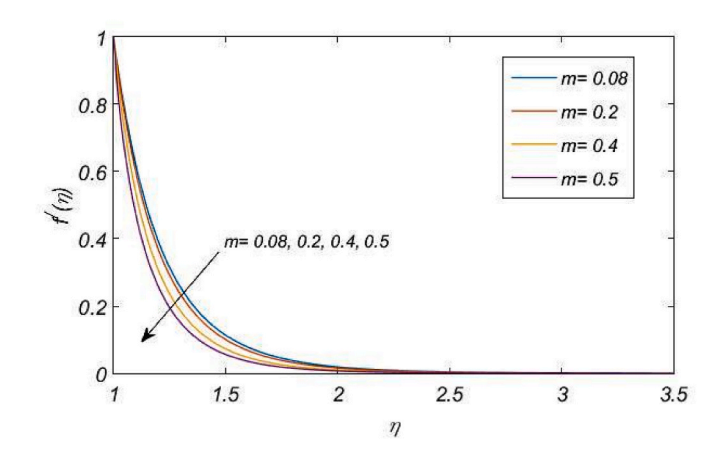


Fig. 2. Illustration of velocity curve for distinct values of m

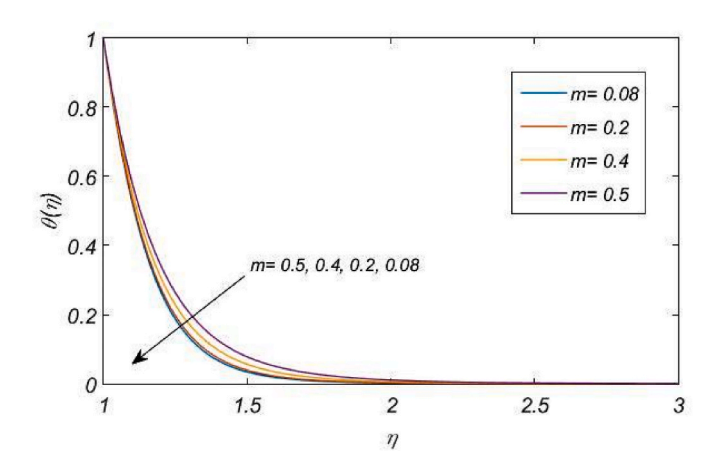


Fig. 3. Illustration of the thermal curve for distinct values of m

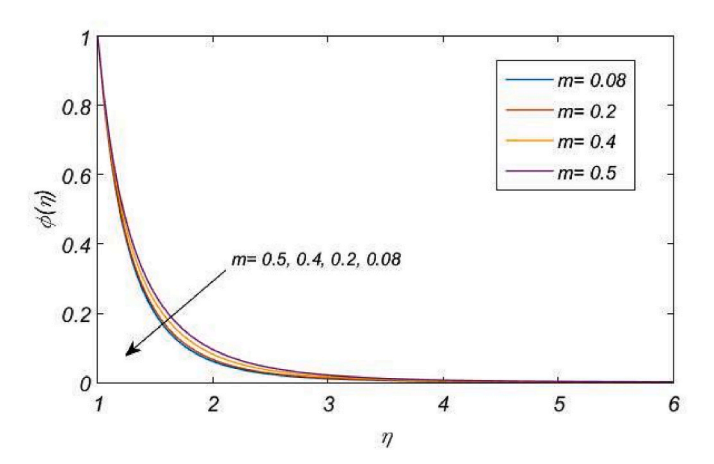


Fig. 4. Illustration of concentration curve for distinct values of m

$$\frac{\sigma_{hnf}}{\sigma_f} = \left\{ \frac{\sigma_{s2} + 2\sigma_{nf} - 2\phi_2(\sigma_{nf} - \sigma_{s2})}{\sigma_{s2} + 2\sigma_{nf} + \phi_2(\sigma_{nf} - \sigma_{s2})} \right\}$$

3. Method of the solution

Using MATLAB's bvp4c function, we numerically solved the coupled higher-order ODEs (6)–(8), defined by boundary conditions in equations (9) and (10), across a specified range of physical variable values. This solver, designed for boundary value problems, implements the three-stage Lobatto IIIa algorithm within a finite difference framework. For

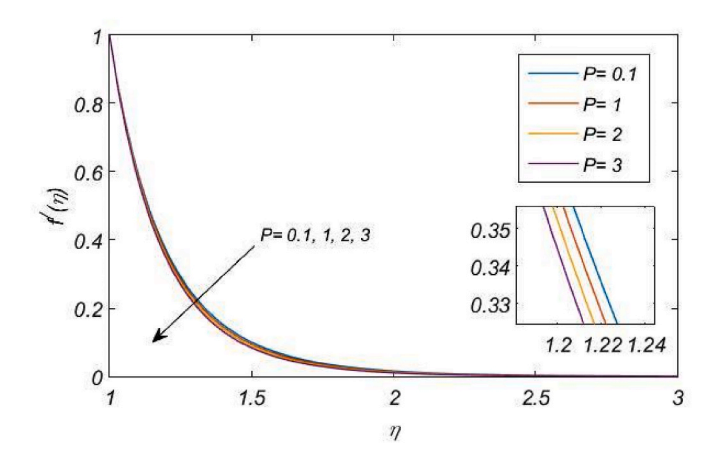


Fig. 5. Illustration of velocity curve for distinct values of P

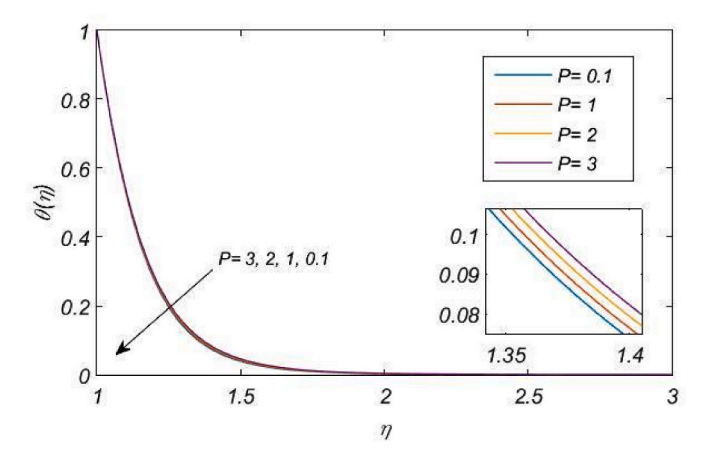


Fig. 6. Illustration of thermal curve for distinct values of P

precise and reliable results, a convergence criterion of 10^{-4} was set, ensuring the solver iterated until the solution accuracy reached this threshold. This approach enabled a comprehensive exploration of the system's behavior, yielding accurate numerical outcomes that align with the physical expectations for the specified parameter range, thus providing a robust basis for analyzing the dynamics under the given boundary constraints.

To employ this methodology, Equations (6)–(8) have been transformed into the following sets of first-order ODEs.

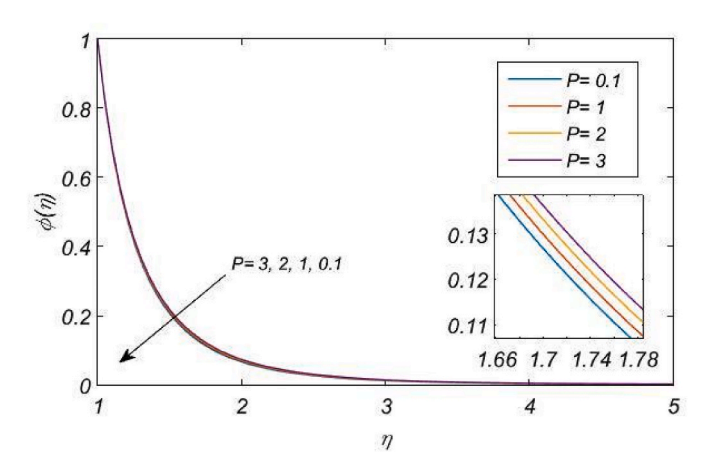


Fig. 7. Illustration of concentration curve for distinct values of P

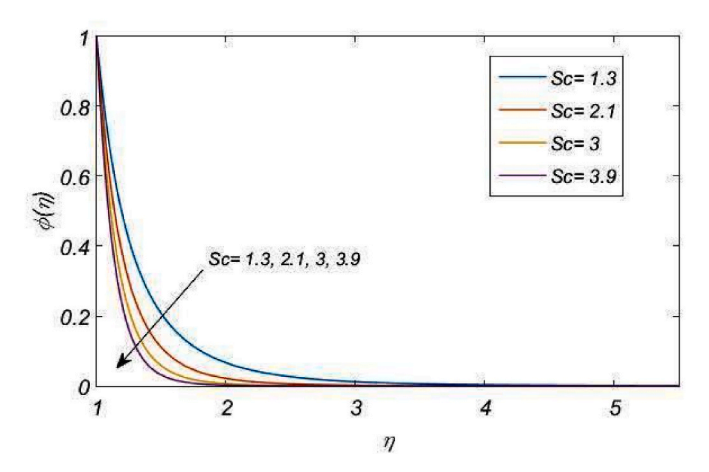


Fig. 8. Illustration of concentration curve for distinct values of Sc

Where, $(y_1, y_2, y_3, y_4, y_5, y_6, y_7)^T = (f, f', f'', \theta, \theta', \phi, \phi')^T$ and $A_1 = \frac{\rho_{lmf}}{\rho_f}$, $A_2 = \frac{\mu_f}{\mu_{lmf}}$, $A_3 = \frac{\sigma_{lmf}}{\sigma_f}$, $A_4 = \frac{(\rho c_p)_{lmf}}{(\rho c_p)_f}$, $A_5 = \frac{k_{lmf}}{k_f}$. Shampine et al. [53] and Dey et al. [54] elaborate on a discussion of this approach.

4. Validation of the findings

The approach employed throughout this investigation has been illustrated to be accurate and precise, as demonstrated by Table 2. By

$$\begin{pmatrix} y_{1}^{'} \\ y_{2}^{'} \\ y_{3}^{'} \\ y_{4}^{'} \\ y_{5}^{'} \\ y_{6}^{'} \\ y_{7}^{'} \end{pmatrix} = \begin{pmatrix} \frac{1}{((1\text{-m})\eta + \text{m.We.}\eta^{\frac{3}{2}}.y_{3})} A_{2}A_{1}Re \\ \frac{1}{((1\text{-m})\eta + \text{m.We.}\eta^{\frac{3}{2}}.y_{3})} A_{2}A_{1}Re \\ \frac{1}{\chi_{2}^{2}} A_{2}A_{1}A_{3} \\ \frac{1}{A_{1}} \\ \frac{1}{A_{1}} \\ \frac{1}{\eta} \left(\frac{1}{1 + \epsilon y_{4}} A_{4} \frac{1}{A_{5}} \left(\Pr{Re} \begin{pmatrix} y_{5} \\ y_{2} y_{4} - y_{1}y_{5} \\ y_{7} \\ y_{7} \\ \end{pmatrix} - \epsilon \cdot \eta \cdot y_{5}^{2} \right) - y_{5} \\ \frac{1}{\eta} \left(\operatorname{Re.Sc} \left(\operatorname{Cr} \left((1 + \gamma y_{4})^{N} \right) e^{\frac{-E}{1 + \gamma y_{4}}} y_{6} + y_{2}y_{6} - y_{1}y_{7} \right) - y_{7} \right) \\ \end{pmatrix}$$

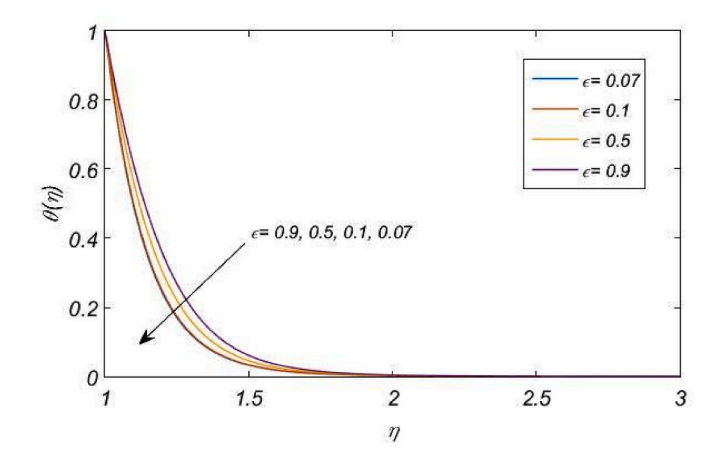


Fig. 9. Illustration of thermal curve for distinct values of ϵ

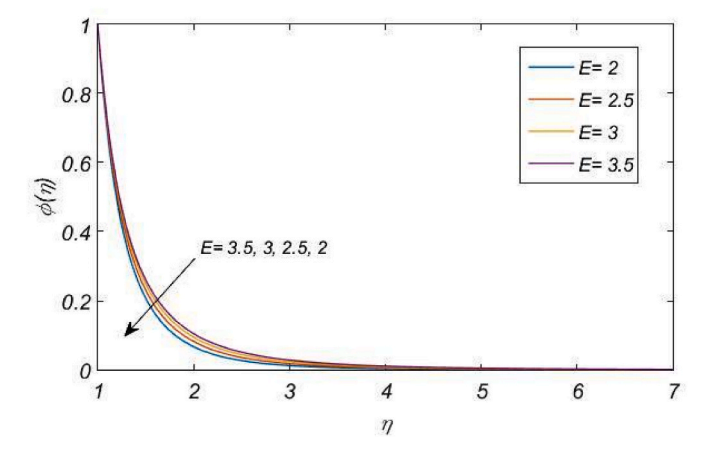


Fig. 10. Illustration of concentration curve for distinct values of E

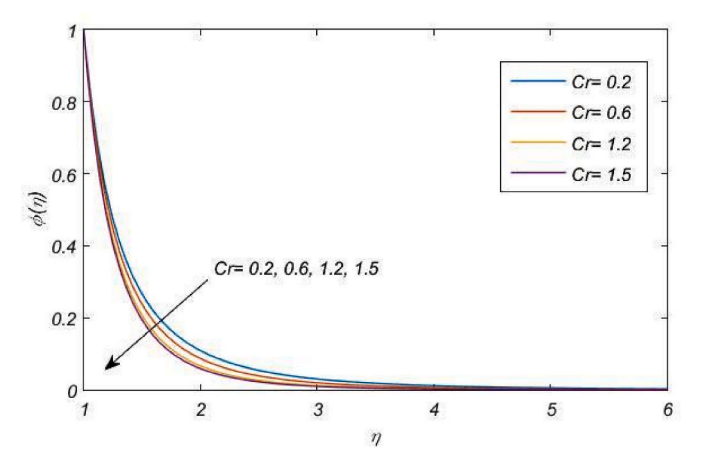


Fig. 11. Illustration of concentration curve for distinct values of Cr

ignoring the mass and energy equation, and neglecting the few physical factors from the momentum equation, the present research is compared with the findings of Wang [55] and Ishak et al. [56]. Hence, the method is reliable, as indicated by the computed results of the present investigation approaching the prior findings.

Also, Table 3 is presented for the meticulous investigation of different experimental studies on the thermal transport properties of nanofluids composed of Ag, and MoS_2 nanoparticles. The in-table references imply that in each of these studies, as spitted out evidence, heat

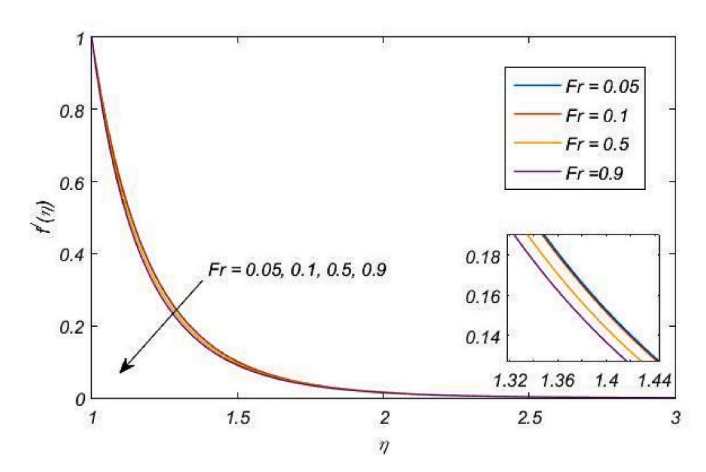


Fig. 12. Illustration of velocity curve for distinct values of Fr

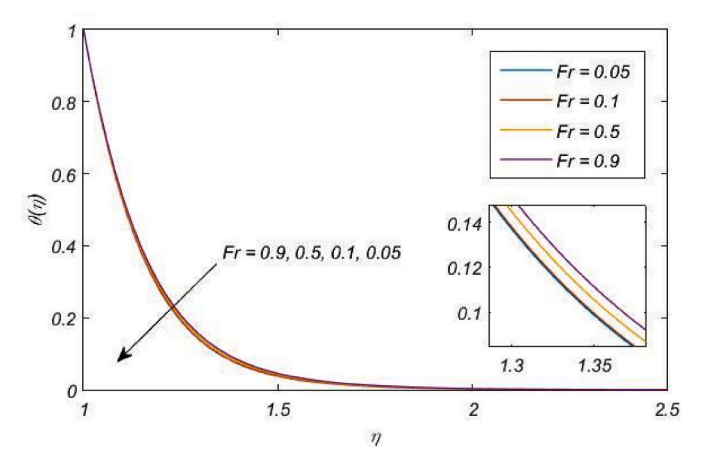


Fig. 13. Illustration of the thermal curve for distinct values of Fr

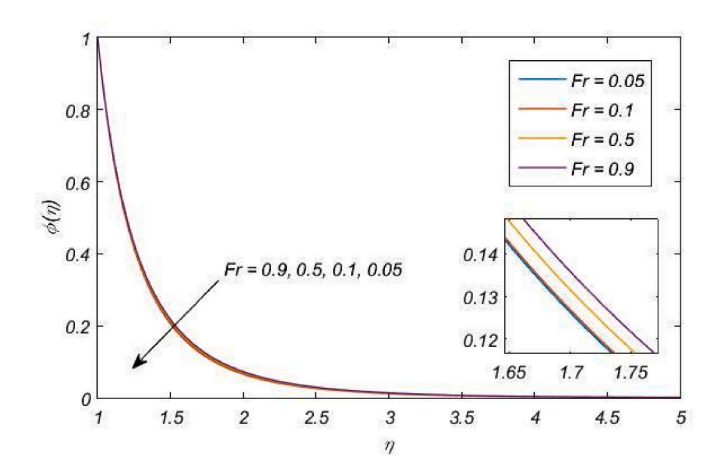


Fig. 14. Illustration of concentration curve for distinct values of Fr

transmission was indeed highly amplified in the developed nanofluids. These selected investigations ascertain the relatively strong thermal conductivity of nanoparticles and convective heat transfer phenomenon on the synthesized Ag, and MoS_2 nanofluidic. From the collected data, the outcome was quite consistent with this review, which stated that silver nanoparticles greatly enhance the thermophysical potential of base fluids for advanced thermal-based applications.

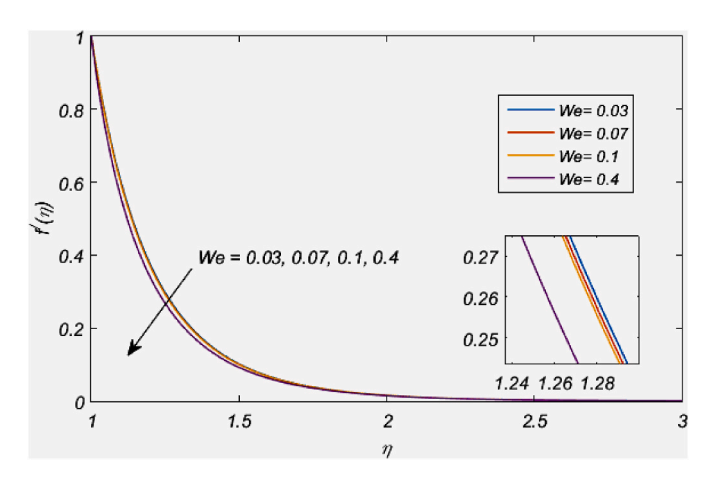


Fig. 15. Illustration of velocity curve for distinct values of We

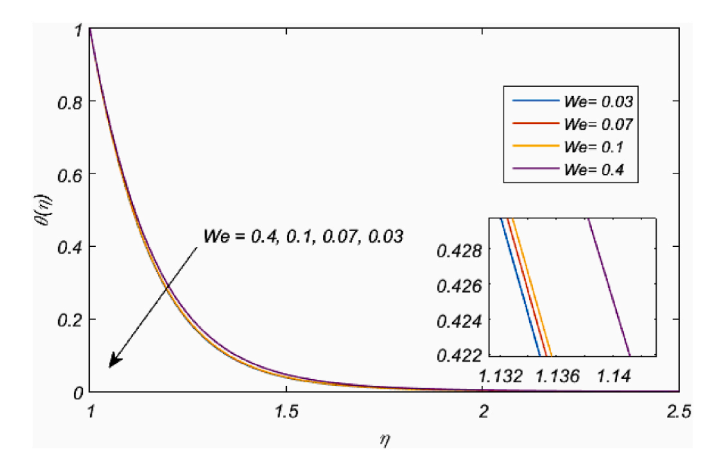


Fig. 16. Illustration of the thermal curve for distinct values of We

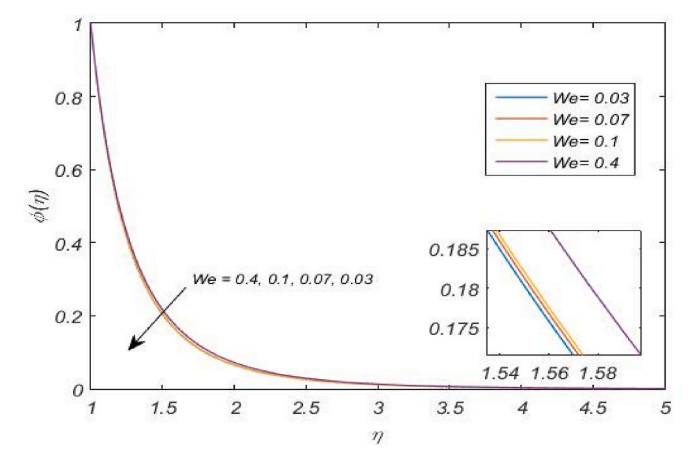


Fig. 17. Illustration of the concentration curve for distinct values of We

5. Result and discussion

The MHD tangent hyperbolic $Ag-MoS_2$ /water Williamson hybrid nanofluid flow incorporating the activation energy, chemical reaction, variable thermal conductivity, and Darcy-Forchheimer impacts over an exponentially stretched cylinder is addressed in this manuscript. The repercussions of various dimensionless variables on the velocity, heat, and concentration curves are portrayed in graphs (Figs. 2–17).

In this investigation, the values of the dimensionless factors depend

on the rheological features of the base fluid, and the nanoparticles are kept constant based on the rheological features of the hybrid nanofluid as $Pr=7, m=0.2, Re=10, M=0.9, P=0.1, N=3, Sc=1.3, \gamma=0.2, \epsilon=0.3, E=2, Cr=1.2, Fr=0.1$, and We=0.1, when required, and the findings are analyzed accordingly. Furthermore, as shown by Paul et al. [47], some parameter values have been considered.

The volume fraction of Ag and MoS_2 is considered as 0.05 % and 0.08 % respectively, immersed in the water. So, the total volume percentage of nanoparticles is 0.13 %. It is done because more nanoparticle volume percentage may create agglomeration, which in turn hampers the fluidity. As a result, the fluid's characteristics are ensured to be minimally affected by the nanoparticles. This volume ratio is maintained throughout the whole flow problem investigation. Moreover, the shear rate, thermal, and mass transmission are displayed in the tables. The coupled non-linear ODEs (6)–(8) are solved employing the finite difference in-built MATLAB code Bvp4c in compliance with the boundary constraints (9) and (10), notch the computational findings.

In Fig. 2, the velocity curve reduces as the tangent hyperbolic factor (*m*) is elevated. Since the shear-thinning tendency is stronger when the tangent hyperbolic factor rises, the fluid's effective viscosity also upsurges. A diminution in the velocity profile results from this advanced flow resistance. Also in Figs. 3 and 4, it has been noticed that boosting the values of tangent hyperbolic factor (*m*), enhanced both thermal and concentration curves respectively. A higher tangent hyperbolic factor upsurges the fluid's resistance to deformation, which consequences in lesser momentum transmission and superior energy dissipation. By enhancing the thermal and concentration boundary layers, this elevated resistance escalates the thermal and concentration profiles.

The impacts of the porosity term (P), on the fluid velocity is demonstrated in Fig. 5. It comes to light that as P improves, the fluid's flow diminishes. There is a converse correlation between the porosity factor P and the porous space diameter k_p . As a consequence, when P climb, the porous space diameter is lessened, which provides a stumbling block in the path of the flow. Due to this obstruction, the velocity of the fluid has been slowed down in Fig. 5, but the thermal profile reflected the opposite trend as P developed in Fig. 6. The significance of the porosity factor P on the non-dimensional concentration curves is depicted in Fig. 7. As the porosity parameter P improves the concentration profile mounts as well. This occurs because the escalating viscosity hinders fluid motion, and so the concentration curve is augmented.

Fig. 8 illustrates that there is a significant reduction in concentration distribution with an upsurge in Schmidt number (Sc). As the Schmidt number (Sc) escalates, the mass diffusivity of the solute shrinks, restraining its diffusion within the fluid. This lessening in diffusivity leads to a thinner concentration boundary layer, resulting in an inferior concentration profile.

The influence of varying thermal conductivity factor (ϵ) on thermal distribution is portrayed in Fig. 9. It has been visualized from the plot that enhanced the value of ϵ results in improving the thermal curve. Enhancing the varying thermal conductivity factor augments thermal conduction within the fluid, consenting to more efficient thermal transmission. This enhancement advances the thermal profile, as heat energy is more readily dispersed throughout the medium.

Fig. 10 illuminates the improving pattern of activation energy (*E*) on the concentration curve. The reaction rate falls as the activation energy upsurges because fewer molecules have enough energy to cross the energy barrier. Comparing this slower reaction rate to reactions with lower activation energy, the concentration of the reactant declines more gradually over time, resulting in a better concentration curve.

Fig. 11 demonstrates how the concentration profile gradually drops as the chemical reaction factor boosts. The cause of the concentration field reduction is that as the chemical reaction factor escalates, the magnitude of solute molecules performing the reaction also augments, which causes a decline in the field of concentration.

Figs. 12–14 demonstrate the importance of the Darcy–Forchheimer

Table 4 Computed findings for various physical components while $\phi_1=0.05$ and $\phi_2=0.08$

m	P	Sc	ϵ	E	Cr	Fr	We	Skin Friction	Nusselt Number	Sherwood Number
0.08	0.1	1.3	0.3	2	1.2	0.1	0.1	-6.2476	26.9860	4.1047
0.2								-5.6139	26.6112	4.0459
0.4								-4.4567	25.4617	3.8843
0.5								-3.4640	24.0769	3.7222
	0.1							-5.6139	26.6112	4.0459
	1							-5.7110	26.4954	4.0262
	2 3							-5.8157	26.3706	4.0059
	3							-5.9172	26.2493	3.9864
		1.3						-5.6139	26.6112	4.0459
		2.1						-5.6139	26.6112	5.3827
		3						-5.6139	26.6112	6.6221
		3.9						-5.6139	26.6112	7.6906
			0.1					-5.6139	29.9076	4.0356
			0.5					-5.6139	24.1091	4.0553
			0.7					-5.6139	22.1320	4.0639
			0.9					-5.6139	20.5220	4.0720
				2				-5.6139	26.6112	4.0459
				2.5				-5.6139	31.0464	3.8209
				3				-5.6139	35.4816	3.6656
				3.5				-5.6139	39.9168	3.5605
					0.2			-5.6139	26.6112	3.4972
					0.6			-5.6139	26.6112	3.7339
					1.2			-5.6139	26.6112	4.0459
					1.5			-5.6139	26.6112	4.1895
						0.05		-5.5598	26.6512	4.0515
						0.1		-5.6139	26.6112	4.0459
						0.5		-6.0284	26.3053	4.0036
						0.9		-6.4154	26.0213	3.9654
							0	-5.7383	26.7127	4.0599
							0.1	-5.6677	26.6562	4.0521
							0.1	-5.6139	26.6112	4.0459
							0.4	-5.0006	25.9396	3.9591

Table 5
Computed Skin friction coefficient, Nusselt number, and Sherwood number for nanofluid, hybrid-nanofluid and Williamson hybrid nanofluid

Fluid	We	ϕ_1	ϕ_2	Skin friction	Nusselt Number	Sherwood Number
Nanofluid	0	0.02 0.05 0.07	0	-4.4700 -5.0293 -5.4140	23.9990 24.5542 24.9249	4.0100 3.9817 3.9686
Hybrid nanofluid	0	0.09 0.02 0.05 0.07	0.08	-5.8107 -5.2107 -5.7906 -6.1924	25.2973 26.1137 26.7527 27.1790	3.9592 4.0817 4.0656 4.0589
Williamson hybrid nanofluid	0.1	0.09 0.02 0.05 0.07 0.09	0.08	-6.6087 -5.0551 -5.6139 -6.0013 -6.4029	27.6070 25.9890 26.6112 27.0267 27.4445	4.0550 4.0626 4.0459 4.0389 4.0349

inertia component, Fr. Remarkably, fluid velocity declines as the Darcy-Forchheimer factor (Fr) improves as the inertia factor has a correlation to the drag coefficient and the permeability of the medium. As a consequence, both the medium's porosity and drag coefficient are enhanced with climbing C_b . So the resistive force of the liquid boosts which leads to a reduction in velocity with an elevated Forchheimer number. Similar findings in stretching sheets were found by Paul et al. [55] in their recent research. Also in Figs. 13 and 14, while the Darcy-Forchheimer factor (Fr) enhances, an elevation in the thermal as well as the concentration curve has been illustrated. Greater inertial impacts in the fluid movement are indicated by an increasing Darcy-Forchheimer factor, which results in elevated resistance to fluid flow. This higher resistance slows down the mixing and transit of thermal energy and species concentration by reducing convective thermal and mass transmission. The temperature and concentration profiles thus become more noticeable close to the surface as diffusion takes precedence over convection.

The correlation between fluid velocity and the Weissenberg number (We) is presented in Fig. 15, and it is evident that the velocity curve reduces as the Weissenberg number elevates. This is due to boosting Weissenberg number values, which strengthen viscosity, improve resistance to fluid flow, and diminish fluid velocity. The influence of the Weissenberg number on the temperature curve is demonstrated in Fig. 16. While the Weissenberg number goes up, so does the thermal profile. As the Weissenberg number grows, fluid movement displays enhanced elastic impacts that promote fluid stretching and internal friction-induced energy dissipation. Because of the supplementary heat produced by this superior dissipation, the fluid's temperature upsurges, enlightening the thermal profile. Also, in Fig. 17, as the Weissenberg number enhances the concentration profile also escalates. An elevated Weissenberg number amplifies elastic stresses, which improve fluid stretching and convective movement. This raises the concentration profile through enhanced particle alignment and accumulation.

Table 4 points out the effect of dimensionless variables on the coefficient of skin friction, and the thermal and mass transmission rate. It has been observed that the surface's absolute rate of shear stress is enhanced with the boosting values of the porosity factor (P) and Darcy–Forchheimer factor (Fr), but a declination of the absolute rate of friction drag is notably observed for the tangent hyperbolic factor (m) and Weissenberg number (We). Also, the Sherwood number appears to upsurge with surging values of the non-dimensional elements Schmidt number (Sc), Variable conductivity factor (ϵ) and chemical reaction term (Cr). On the other hand, except for the growing values of activation energy factor (E), the thermal transmission rate is found to be reduced for enhancing tangent hyperbolic factor (m), Porosity factor (P), Variable conductivity factor (ϵ) , Darcy–Forchheimer factor (Fr), and Weissenberg number (We).

Table 5 exhibits that, although the volume fraction of MoS_2 is maintained at zero, a hike in the volume fraction of Ag nanoparticles sstrengthens both absolute skin friction and heat transfer rate, but the Sherwood number decreases. Additionally, it is worth mentioning that

the hybrid nanofluid exhibited an upsurge in the absolute shear stress rate of up to $16.5\,\%$ in comparison to nanofluid and a boost in the rate of heat transportation of more than $8.8\,\%$, despite the solid volume proportion of MoS_2 being maintained at 0.08. Also, it has been notably noticed that in comparison to the Williamson hybrid nanofluid, the hybrid nanofluid indicates an enhancement of up to $3.2\,\%$ in terms of absolute skin friction coefficient. From the aforementioned findings, it is unambiguous that the hybrid nanofluid has notably greater mass and thermal transmission rates than both the nanofluid and Williamson hybrid nanofluid. Those outcomes have a variety of industrial and engineering applications.

6. Conclusion

In this present exploration, we have investigated the MHD $Ag-MoS_2/H_2O$ Williamson hybrid nanofluid flow in Darcy-Forchheimer permeable media incorporating variable thermal conductivity over an exponentially stretched cylinder. By integrating the activation energy and chemical reaction, the flow model's uniqueness is reinforced. The numerical findings are obtained by MATLAB Bvp4c algorithm for the non-dimensional flow model. The implications of distinct terms on velocity, heat, concentration curves, rate of shear stress, rate of mass, and thermal transport are inspected and demonstrated through graphs and tables. The noteworthy outcomes of this research are enlisted as follows:

- > The velocity of the fluid is a declining function of the Weissenberg number, Porosity term, tangent hyperbolic factor, and Darcy-Forchheimer factor respectively.
- > Schmidt number and chemical reaction factor, respectively, have a diminishing influence on concentration. But enhancing the function of activation energy, tangent hyperbolic factor, and Darcy-Forchheimer factor respectively.
- > The thermal curve escalates for elevating Weissenberg number, Darcy-Forchheimer, tangent hyperbolic, varying thermal conductivity, and porosity factor.
- > The rate of thermal transport is found to decline for enhancing tangent hyperbolic factor, porosity, varying thermal conductivity, Darcy-Forchheimer factor, and Weissenberg number Also, the rate of mass transport appears to enhance with boosting values of the non-

- dimensional components Schmidt number, chemical reaction factor and varying thermal conductivity term.
- ➤ The hybrid nanofluid displays an enrichment in the absolute rate of shear stress of up to 3.2 % compared to the Williamson hybrid nanofluid.
- > The hybrid nanofluid has significantly greater mass and thermal transport rates than both the nanofluid and Williamson hybrid nanofluid.

These outcomes open up extensive real-world utilizations in domains, such as the automotive industry, solar thermal structures, microfluidics, medical apparatus, and nuclear reactors that depend on effective thermal and mass transmission. Also, Williamson hybrid nanofluids exhibit a variety of fascinating rheological behaviors that may lead to significant new insights into intricate fluid dynamics and thermal transport mechanisms.

CRediT authorship contribution statement

Jintu Mani Nath: Writing – original draft, Methodology, Investigation, Conceptualization. Tusar Kanti Das: Methodology, Conceptualization. Ashish Paul: Writing – review & editing and Supervision. Ali J. Chamkha: Writing – review & editing.

Data availability statement

All data that support the findings of this study are included within the article.

Financial interests

Authors have no financial interests.

Declaration of competing interest

The authors have declared that they have no conflicts of interest related to this study. Furthermore, there is no funding agency associated with the study design or manuscript preparation.

NOMENCLATURE:

- T Temperature of the fluid
- T_w Temperature at the wall
- T_{∞} Ambient fluid temperature
- C Concentration of hybrid nanofluid
- C_w The concentration of hybrid nanofluid at the wall
- C_{∞} Ambient concentration of hybrid nanoparticle
- D Mass diffusivity
- m Tangent hyperbolic factor
- We Weissenberg number
- M Magnetic parameter
- *E* Activation energy factor
- Pr Prandtl number
- Sc Schmidt number
- Re Reynolds number
- N Proportionality ratio parameter
- Fr Darcy-Forchheimer factor
- P Porosity Parameter
- Variable conductivity parameter
- Cr Chemical reaction parameter
- γ Temperature ratio parameter
- *B*₀ Dimensional magnetic field
- ϕ_1 Concentration of 1st nanoparticle

 $\begin{array}{ll} \phi_2 & \text{Concentration of 2nd nanoparticle} \\ \rho_{s1} & \text{Density of 1st solid particle } (\textit{Ag}) \\ \rho_{s2} & \text{Density of 2nd solid particle } (\textit{MoS}_2) \end{array}$

 ρ_f Density of the base fluid

 $(\rho c_p)_{s1}$, $(\rho c_p)_{s2}$ Specific heat capacity of 1st and 2nd solid particle

 $egin{array}{ll} \left(
ho c_p
ight)_f & ext{Base fluid-specific heat capacity} \\ k_f & ext{Thermal Conductivity of base Fluid} \end{array}$

 k_{s1}, k_{s2} Thermal Conductivity of 1st and 2nd solid particle σ_{s1}, σ_{s2} The electric conductivity of 1st and 2nd solid particle

 σ_f Base fluid electric conductivity

 c_b Drag coefficient α_f Thermal diffusivity

k_p Dimensional porosity factor

 k_r Dimensional chemical reaction factor

References

- [1] N. Bachok, A. Ishak, I. Pop, Boundary layer stagnation-point flow and heat transfer over an exponentially stretching/shrinking sheet in a nanofluid, Int. J. Heat Mass Tran. 55 (25–26) (2012) 8122–8128.
- [2] C.Y. Wang, Fluid flow due to a stretching cylinder, Phys. Fluid. 31 (3) (1988) 466–468.
- [3] I. Khan, S. Ullah, M.Y. Malik, A. Hussain, Numerical analysis of MHD Carreau fluid flow over a stretching cylinder with homogenous-heterogeneous reactions, Results Phys. 9 (2018) 1141–1147.
- [4] R.N. Kumar, R.P. Gowda, A.M. Abusorrah, Y.M. Mahrous, N.H. Abu-Hamdeh, A. Issakhov, B.C. Prasannakumara, Impact of magnetic dipole on ferromagnetic hybrid nanofluid flow over a stretching cylinder, Phys. Scripta 96 (4) (2021) 045215.
- [5] A. Paul, T.K. Das, J.M. Nath, Numerical investigation on the thermal transportation of MHD Cu/Al 2 O 3-H 2 O Casson-hybrid-nanofluid flow across an exponentially stretching cylinder incorporating heat source, Phys. Scripta 97 (8) (2022) 085701.
- [6] A. Othman, H, B. Ali, S. Jubair, M. Yahya Almusawa, M. Aldin, S, Numerical simulation of the nanofluid flow consists of gyrotactic microorganism and subject to activation energy across an inclined stretching cylinder, Sci. Rep. 13 (1) (2023) 7719
- [7] S. Li, M.I. Khan, S.U. Khan, S. Abdullaev, M.M.I. Mohamed, M.S. Amjad, Effectiveness of melting phenomenon in two phase dusty carbon nanotubes (Nanomaterials) flow of Eyring-Powell fluid: heat transfer analysis, Chin. J. Phys. 86 (2023) 160–169.
- [8] Zeeshan, N.A. Ahammad, N.A. Shah, J.D. Chung, Role of nanofluid and hybrid nanofluid for enhancing thermal conductivity towards exponentially stretching curve with modified Fourier law inspired by melting heat effect, Mathematics 11 (5) (2023) 1170.
- [9] S. Li, M. Imtiaz, M. Ijaz Khan, R.N. Kumar, K.S. Akramova, Applications of Soret and Dufour effects for Maxwell nanomaterial by convectively heated surface, Numer. Heat Tran., Part A: Applications (2024) 1–15.
- [10] M.M. Maskeen, A. Zeeshan, O.U. Mehmood, M. Hassan, Heat transfer enhancement in hydromagnetic alumina–copper/water hybrid nanofluid flow over a stretching cylinder, J. Therm. Anal. Calorim. 138 (2019) 1127–1136.
- [11] H. Waqas, S.M.R.S. Naqvi, M.S. Alqarni, T. Muhammad, Thermal transport in magnetized flow of hybrid nanofluids over a vertical stretching cylinder, Case Stud. Therm. Eng. 27 (2021) 101219.
- [12] N.A. Zainal, R. Nazar, K. Naganthran, I. Pop, Unsteady MHD hybrid nanofluid flow towards a horizontal cylinder, Int. Commun. Heat Mass Tran. 134 (2022) 106020.
- [13] A. Paul, J. Mani Nath, T. Kanti Das, An investigation of the MHD Cu-Al 2 O 3/H 2 O hybrid-nanofluid in a porous medium across a vertically stretching cylinder incorporating thermal stratification impact, J. Therm. Eng. 9 (3) (2023).
- [14] S. Nandi, D. Barman, Unsteady MHD hybrid nanofluid flow over a convectively heated linear stretching cylinder with velocity slip: a comparative study, Int. J. Mod. Phys. B (2023) 2450284.
- [15] S.S.P.M. Isa, S. Parvin, N. Arifin, F. Ali, K. Ahmad, Soret-Dufour effects on the waterbased hybrid nanofluid flow with nanoparticles of Alumina and Copper, Malaysian J Math Sci 15 (19) (2023) 3419.
- [16] S. Li, A. Abbasi, W. Farooq, M. Gul, M.I. Khan, G. Nafasova, H.A. Hejazi, Heat and mass transfer characteristics of Al2O3/H2O and (Al2O3+ Ag)/H2O nanofluids adjacent to a solid sphere: a theoretical study, Numer. Heat Tran., Part A: Applications (2024) 1–19.
- [17] Z. Mahmood, K. Rafique, U. Khan, T. Muhammad, T. Alballa, H.A.E.W. Khalifa, Heat transfer in radiative hybrid nanofluids over moving sheet with porous media and slip conditions: numerical analysis of variable viscosity and thermal conductivity, Mater. Today Commun. 40 (2024) 109664.
- [18] S. Mukhopadhyay, MHD boundary layer slip flow along a stretching cylinder, Ain Shams Eng. J. 4 (2) (2013) 317–324.
- [19] Y.D. Reddy, B.S. Goud, K.S. Nisar, B. Alshahrani, M. Mahmoud, C. Park, Heat absorption/generation effect on MHD heat transfer fluid flow along a stretching cylinder with a porous medium, Alex. Eng. J. 64 (2023) 659–666.

- [20] X. Zhou, M.A. Qureshi, N. Khan, W. Jamshed, S.S.P. Mohamed Isa, N. Balakrishnan, S.M. Hussain, Thermosolutal Marangoni convective flow of MHD tangent hyperbolic hybrid nanofluids with elastic deformation and heat source, Open Phys. 22 (1) (2024) 20240082.
- [21] S.S.P.M. Isa, H.M. Azmi, N. Balakrishnan, A.S.M. Nazir, K. Ahmad, N.S. Ismail, H. Rosali, The soret-dufour effects on three-dimensional magnetohydrodynamics Newtonian fluid flow over an inclined plane, CFD Lett. 16 (9) (2024) 39–51.
- [22] R.V. Williamson, The flow of pseudoplastic materials, Ind. Eng. Chem. 21 (11) (1929) 1108–1111.
- [23] M. Bilal, M. Sagheer, S. Hussain, Numerical study of magnetohydrodynamics and thermal radiation on Williamson nanofluid flow over a stretching cylinder with variable thermal conductivity, Alex. Eng. J. 57 (4) (2018) 3281–3289.
- [24] W. Ibrahim, M. Negera, The investigation of MHD Williamson nanofluid over stretching cylinder with the effect of activation energy, Advances in Mathematical Physics 2020 (2020) 1–16.
- [25] X. Zhang, D. Yang, M.I.U. Rehman, A.A. Mousa, A. Hamid, Numerical simulation of bioconvection radiative flow of Williamson nanofluid past a vertical stretching cylinder with activation energy and swimming microorganisms, Case Stud. Therm. Eng. 33 (2022) 101977.
- [26] A.M. Rashad, M.A. Nafe, D.A. Eisa, Heat variation on MHD Williamson hybrid nanofluid flow with convective boundary condition and Ohmic heating in a porous material, Sci. Rep. 13 (1) (2023) 6071.
- [27] T. Salahuddin, M.Y. Malik, A. Hussain, M. Awais, I. Khan, M. Khan, Analysis of tangent hyperbolic nanofluid impinging on a stretching cylinder near the stagnation point, Results Phys. 7 (2017) 426–434.
- [28] P.P. Gharami, S. Reza-E-Rabbi, S.M. Arifuzzaman, M.S. Khan, T. Sarkar, S. F. Ahmmed, MHD effect on unsteady flow of tangent hyperbolic nano-fluid past a moving cylinder with chemical reaction, SN Appl. Sci. 2 (2020) 1–16.
- [29] P. Kumar, H. Poonia, L. Ali, S. Areekara, The numerical simulation of nanoparticle size and thermal radiation with the magnetic field effect based on tangent hyperbolic nanofluid flow, Case Stud. Therm. Eng. 37 (2022) 102247.
- [30] P.M. Patil, B. Goudar, M.A. Sheremet, Tangent hyperbolic ternary hybrid nanofluid flow over a rough-yawed cylinder due to impulsive motion, J. Taibah Univ. Sci. 17 (1) (2023) 2199664.
- [31] A. Saeed, A. Tassaddiq, A. Khan, M. Jawad, W. Deebani, Z. Shah, S. Islam, Darcy-Forchheimer MHD hybrid nanofluid flow and heat transfer analysis over a porous stretching cylinder, Coatings 10 (4) (2020) 391.
- [32] A.K. Gautam, A.K. Verma, K. Bhattacharyya, S. Mukhopadhyay, A.J. Chamkha, Impacts of activation energy and binary chemical reaction on MHD flow of Williamson nanofluid in Darcy–Forchheimer porous medium: a case of expanding sheet of variable thickness, Waves Random Complex Media (2021) 1–22.
- [33] I. Haq, M.F. Yassen, M.E. Ghoneim, M. Bilal, A. Ali, W. Weera, Computational Study of MHD Darcy–Forchheimer hybrid nanofluid flow under the influence of chemical reaction and activation energy over a stretching surface, Symmetry 14 (9) (2022) 1759.
- [34] A.M. Alqahtani, M. Bilal, M. Usman, T.R. Alsenani, A. Ali, S.R. Mahmuod, Heat and mass transfer through MHD Darcy Forchheimer Casson hybrid nanofluid flow across an exponential stretching sheet, ZAMM-Journal of Applied Mathematics and Mechanics/ZeitschriftfürAngewandteMathematik und Mechanik (2023) e202200213.
- [35] S. Li, M.I. Khan, S. Ali, S. Ullah Khan, S.A. Althobaiti, I. Khan, M. Kchaou, Influence of variable fluid properties on mixed convective Darcy–Forchheimer flow relation over a surface with Soret and Dufour spectacle, Open Phys. 22 (1) (2024) 20240010.
- [36] S. Enamul, S. Ontela, Magnetohydrodynamic Darcy-Forchheimer flow of non-Newtonian second-grade hybrid nanofluid bounded by double-revolving disks with variable thermal conductivity: Entropy generation analysis, Hybrid Advances (2024) 100226.
- [37] M. Shanmugapriya, R. Sundareswaran, P. Senthil Kumar, Heat and mass transfer enhancement of MHD hybrid nanofluid flow in the presence of activation energy, Int. J. Chem. Eng. 2021 (2021) 1–12.

- [38] M. Azam, Non-linear radiative heat flux of Williamson nanofluid with gyrotactic microorganisms, activation energy and bioconvection, Waves Random Complex Media (2022) 1–23.
- [39] P. Kumar, H. Poonia, S. Areekara, A.S. Sabu, A. Mathew, L. Ali, Significance of irregular heat source and Arrhenius energy on electro-magnetohydrodynamic hybrid nanofluid flow over a rotating stretchable disk with nonlinear radiation, Numer. Heat Tran., Part A: Applications (2023) 1–23.
- [40] V. Puneeth, S. Manjunatha, M.S. Anwar, M. Oreijah, K. Geudri, O.T. Bafakeeh, A. M. Galal, Stratified bioconvective jet flow of Williamson nanofluid in porous medium in the presence of Arrhenius activation energy, Journal of Computational Biophysics and Chemistry 22 (3) (2023) 309–319.
- [41] S.K. Saini, R. Agrawal, P. Kaswan, Activation energy and convective heat transfer effects on the radiative Williamson nanofluid flow over a radially stretching surface containing Joule heating and viscous dissipation, Numer. Heat Tran., Part A: Applications (2023) 1–24.
- [42] S. Li, M.I. Khan, F. Ali, S.S. Abdullaev, S. Saadaoui, Habibullah, Mathematical modeling of mixed convective MHD Falkner-Skan squeezed Sutterby multiphase flow with non-Fourier heat flux theory and porosity, Appl. Math. Mech. 44 (11) (2023) 2005–2018.
- [43] S.S.P.M. Isa, H.M. Azmi, N.M. Arifin, H. Rosali, Soret-dufour effects on heat and mass transfer of Newtonian fluid flow over the inclined sheet and magnetic field, Journal of Advanced Research in Numerical Heat Transfer 14 (1) (2023) 39–48.
- [44] S. Li, C. Rajashekhar, K.S. Nisar, F. Mebarek-Oudina, H. Vaidya, M.I. Khan, G. Manjunatha, Peristaltic transport of a Ree-Eyring fluid with non-uniform complaint channel: an analysis through varying conditions, ZAMM-Journal of Applied Mathematics and Mechanics/Zeitschrift für Angewandte Mathematik und Mechanik 104 (2) (2024) e202300073.
- [45] H. Adun, D. Kavaz, M. Dagbasi, Review of ternary hybrid nanofluid: synthesis, stability, thermophysical properties, heat transfer applications, and environmental effects, J. Clean. Prod. 328 (2021) 129525.
- [46] H. Adun, D. Kavaz, M. Dagbasi, H. Umar, I. Wole-Osho, An experimental investigation of thermal conductivity and dynamic viscosity of Al2O3-ZnO-Fe3O4 ternary hybrid nanofluid and development of machine learning model, Powder Technol. 394 (2021) 1121–1140.
- [47] A. Paul, T.K. Das, Darcy–Forchheimer MHD radiative flow through a porous space incorporating viscous dissipation, heat source, and chemical reaction effect across an exponentially stretched surface, Heat Transfer 52 (1) (2023) 807–825.

- [48] A. Paul, J.M. Nath, T.K. Das, Thermally stratified Cu–Al2O3/water hybrid nanofluid flow with the impact of an inclined magnetic field, viscous dissipation and heat source/sink across a vertically stretching cylinder, ZAMM-Journal of Applied Mathematics and Mechanics/ZeitschriftfürAngewandteMathematik und Mechanik (2023) e202300084.
- [49] T. Hayat, S. Nadeem, Heat transfer enhancement with Ag-CuO/water hybrid nanofluid, Results Phys. 7 (2017) 2317–2324.
- [50] F. Ahmad, H. Waqas, H. Ayed, S. Hussain, S. Farooq, S.A. Khan, A.O. Almatroud, Numerical treatment with Lobatto-IIIa scheme magneto-thermo-natural convection flow of casson nanofluid (MoS2— Cu/SA) configured by a stretching cylinder in porous medium with multiple slips, Case Stud. Therm. Eng. 26 (2021) 101132.
- [51] M. Yaseen, M. Kumar, S.K. Rawat, Assisting and opposing flow of a MHD hybrid nanofluid flow past a permeable moving surface with heat source/sink and thermal radiation, Partial Differential Equations in Applied Mathematics 4 (2021) 100168.
- [52] A. Paul, N. Sarma, B. Patgiri, Thermal and mass transfer analysis of Casson-Maxwell hybrid nanofluids through an unsteady horizontal cylinder with variable thermal conductivity and Arrhenius activation energy, Numer. Heat Tran., Part A: Applications (2023) 1–26.
- [53] L.F. Shampine, J. Kierzenka, M.W. Reichelt, Solving boundary value problems for ordinary differential equations in MATLAB with bvp4c, Tutorial notes 2000 (2000) 1–27.
- [54] B. Dey, J.M. Nath, T.K. Das, D. Kalita, Simulation of transmission of heat on viscous fluid flow with varying temperatures over a flat plate, JP J. Heat Mass Transf. 30 (2022) 1–18.
- [55] C.Y. Wang, Fluid flow due to a stretching cylinder, Phys. Fluid. 31 (3) (1988) 466–468.
- [56] A. Ishak, R. Nazar, I. Pop, Uniform suction/blowing effect on flow and heat transfer due to a stretching cylinder, Appl. Math. Model. 32 (10) (2008) 2059–2066.
- [57] Y. Zhang, C. Li, D. Jia, D. Zhang, X. Zhang, Experimental evaluation of MoS2 nanoparticles in jet MQL grinding with different types of vegetable oil as base oil, J. Clean. Prod. 87 (2015) 930–940.
- [58] S.B. Mousavi, S.Z. Heris, P. Estellé, Viscosity, tribological and physicochemical features of ZnO and MoS2 diesel oil-based nanofluids: an experimental study, Fuel 293 (2021) 120481.
- [59] L. Godson, B. Raja, D.M. Lal, S.J.E.H.T. Wongwises, Experimental investigation on the thermal conductivity and viscosity of silver-deionized water nanofluid, Exp. Heat Tran. 23 (4) (2010) 317–332.